NUMERICAL ANALYSIS OF FEM'S FOR THE VISCOACUSTIC WAVE EQUATION

Fabio Iván Zyserman
CONICET, Instituto de Física de La Plata,
CC 67, 1900 La Plata, Argentina
e-mail:zyserman@fisica.unlp.edu.ar

Keywords: Conforming and nonconforming finite elements, dispersion analysis, viscoacustic equation.

Abstract. *We investigate the numerical dispersive properties of two finite element methods yielding a first order spatial approximation, a nonconforming one (NC-method) and the Q_1 conforming method (C-method) when applied to solve the scalar wave equation in dispersive media in the space-frequency domain. The dispersive properties of the subsurface are simulated via a viscoacustic model yielding a constant quality factor in a given fixed frequency range. The study is performed by constructing and analyzing the numeric dispersion relations, and by evaluating derived quantities such as the frequency dependent normalized attenuation, phase and group velocities. It is observed that the NC-method introduces less numerical anisotropy and dispersion than the C-method. Moreover, for a given fixed frequency, the NC-method nearly halves the number of points per wavelength necessary to reach a given accuracy when calculating the mentioned derived quantities.*

1 INTRODUCTION

We are interested in investigating the dispersion properties of numerical solutions yield by a nonconforming finite element method (NC-method)[1,2] and in comparing them with those of the well-known conforming finite element method using bilinear basis functions (C-method) when solving the scalar wave equation in viscoelastic media. The Helmholtz equation arises from a number of applications; in particular, we are going to consider it within the frame of exploration seismology.

Knowing the dispersive properties of the numerical solution is of practical importance, since an underestimation of their relevance can lead to significant numerical error. The dispersive effects in numerical solutions of the scalar wave equation have been widely investigated,[3–9] although in all cases, the coefficients of the equation were considered real and independent of the frequency, i.e., they are valid in the elastic regime. Real materials, however, not always can be considered to behave this way. It is observed that seismic waves loose energy and change their shape when traveling through the subsurface, so a better model for the materials must be used. In the present effort, we are going to consider a viscoelastic model to account for the dispersive behaviour of the soil. On the other hand, most of the modeling of wave propagation in viscoelastic media is done, as far as we are aware, by finite differences in the time domain,[10–13] for which methods yielding an approximately constant quality factor Q have been developed.[14–17] This situations arose mainly because of the lack of portability of previously developed spectral schemes, and also their lack of flexibility to deal with non-periodic boundary conditions.[11] Consequently, the works devoted to study dispersion properties in viscoacoustics/viscoelasticity deal only with finite differences methods, and moreover, the literature in this area is not vast.[18] and[11] made some studies using only one relaxation mechanism, which does not yield a constant Q over the studied frequency range, and,[19] although modelling viscoelastic materials, used real and frequency independent plane wave and shear moduli for their dispersion analysis.

Working in the space-frequency domain, in Section 2 we start our study presenting the chosen viscoelastic model, which allows us to use a constant quality factor, and a complex and frequency dependent plane wave modulus in the acoustic equation. We follow in the same section deriving the finite element approximations to this equation. In Section 3 we derive both the analytic and numeric dispersion relations. We devote Section 4 to thoroughly analyze the numeric dispersion relations for both finite element methods, and finally in Section 5 we draw our conclusions.

2 THEORETICAL BACKGROUND

2.1 Viscoelasticity

The anelastic behaviour of real earth media, attenuating and dispersing traveling mechanical waves is generally described by means of viscoelastic models, i.e., materials are modelled through their mechanical analogs using springs and dashpots. Since long widely

accepted viscoelastic models are the standard linear solid (SLS), consisting in a spring and a dashpot in series (Maxwell body) connected in parallel to a spring having a spring constant associated to the elastic properties of the material, and its improvement the generalized SLS or GSLS (for a detailed description see[17]), which has a finite number of Maxwell bodies connected in parallel to a spring. Each Maxwell body is also called relaxation mechanism, and is characterized by a pair of parameters τ_ϵ, the strain retardation time and τ_σ, the stress relaxation time, being this two times connected to the constants of the spring and dashpot by simple relations.[20][21] proposed the idea of a continuous distribution of relaxation mechanisms, and developed a viscoelastic model that renders the observed behaviour of a constant quality factor Q for a given frequency range -e.g. the exploration seismology one, 1-200 Hz-. Being this model easily used in the frequency domain,[16] we employ it in this paper.

Following[21,22] we see that whenever $\tau_1^{-1} \ll \omega \ll \tau_2^{-1}$, where $\tau_{1,2}$ are relaxation times characterizing the model, it is possible to describe the behaviour of the compressional plane wave modulus by

$$M(\mathbf{x}, \omega) = \frac{M^r(\mathbf{x})}{A(\omega) - i\, B(\omega)}, \tag{1}$$

where $M^r(\mathbf{x}) \equiv M(\mathbf{x}, 0)$ is its relaxed value and

$$A(\omega) = 1 - \frac{1}{\pi\, Q} \log\left(\frac{1 + \omega^2\, \tau_1^2}{1 + \omega^2\, \tau_2^2}\right),$$

$$B(\omega) = \frac{2}{\pi\, Q}\, \tan^{-1}\left(\frac{\omega\, (\tau_1 - \tau_2)}{1 + \omega^2\, \tau_1\, \tau_2}\right). \tag{2}$$

This expressions are valid only for dry rocks; analogous ones can be obtained using, for example, the dissipative Gassman model for porous media saturated by one or two inmiscible fluids.[23]

2.2 Helmholtz equation

Let us consider a bounded bidimensional isotropic, viscoelastic medium, where we want to model the propagation of compressional waves. The region considered will be called Ω, and its boundary Γ. Working in the frequency domain the governing equations are

$$\frac{-\omega^2}{M(\mathbf{x}, \omega)}\widehat{p}(\mathbf{x}, \omega) - \nabla \cdot \left(\frac{1}{\rho(\mathbf{x})}\nabla\widehat{p}(\mathbf{x}, \omega)\right) = \widehat{f}(\mathbf{x}, \omega), \qquad \mathbf{x} \in \Omega,$$

$$\frac{\partial\widehat{p}(\mathbf{x}, \omega)}{\partial\nu} + i\,\omega\,\alpha(\mathbf{x}, \omega)\,\widehat{p}(x, \omega) = 0, \qquad \mathbf{x} \in \Gamma. \tag{3}$$

Here $\widehat{p}(\mathbf{x}, \omega)$ and $\widehat{f}(\mathbf{x}, \omega)$ are the Fourier transforms of the pressure $p(\mathbf{x}, t)$ and the external source respectively, $\rho(\mathbf{x})$ is the density of the medium, ν is the unit outward normal on Γ

and the coefficient $\alpha(\mathbf{x}, \omega) = X(\mathbf{x}, \omega) - i\, Y(\mathbf{x}, \omega)$, where

$$X(\mathbf{x}, \omega) = C_r \left(2\left(C_r^4 + C_i^4\right)\right)^{-1/2} \left(1 + \left(\left(1 + (C_i/C_r)^4\right)^{1/2}\right)\right)^{1/2},$$

$$Y(\mathbf{x}, \omega) = \frac{C_i^2}{C_r} \left(2\left(C_r^4 + C_i^4\right)\right)^{-1/2} \left(1 + \left(\left(1 + (C_i/C_r)^4\right)^{1/2}\right)\right)^{-1/2}, \qquad (4)$$

and

$$C_r^2 = \frac{M_r(\mathbf{x}, \omega)}{\rho(\mathbf{x})}, \qquad C_i^2 = \frac{M_i(\mathbf{x}, \omega)}{\rho(\mathbf{x})}. \qquad (5)$$

[24] have demonstrated that problem (3) is well posed. Its associated variational formulation is given by[1]

$$-\omega^2 \left(\frac{1}{M}\widehat{p}, \varphi\right) + \left(\frac{1}{\rho}\nabla\widehat{p}, \nabla\varphi\right) + i\omega \left\langle \frac{\alpha}{\rho}\widehat{p}, \varphi \right\rangle_\Gamma = (\widehat{f}, \varphi), \qquad \varphi \in H^1(\Omega). \qquad (6)$$

The solution to this equation belongs to $H^1(\Omega)$, the usual Sobolev space of functions in $L^2(\Omega)$ with first derivatives in $L^2(\Omega)$. We use $(f, g) = \int_\Omega f\overline{g}\, dx$ and $\langle f, \overline{g}\rangle = \int_\Gamma f\overline{g}\, d\Gamma$ to denote the complex $[L^2(\Omega)]^2$ and $[L^2(\Gamma)]^2$ inner products.

We state the nonconforming Galerking procedure to find $\widehat{p}^h$, the approximated solution of Eq. (6), as

$$-\left(\frac{\omega^2}{M}\widehat{p}^h, \varphi\right) + \sum_j \left(\frac{1}{\rho}\nabla\widehat{p}^h, \nabla\varphi\right)_j + i\omega \left\langle\!\!\left\langle \frac{\alpha}{\rho}\widehat{p}^h, \varphi \right\rangle\!\!\right\rangle_\Gamma = (\widehat{f}, \varphi), \quad \varphi \in NC^h, \qquad (7)$$

The notation $\langle\!\langle \cdot, \cdot \rangle\!\rangle$ stands for the approximation of the inner product on the boundary by means of the mid-point rule. The properties of the nonconforming finite element space NC^h are extensively studied in;[1] we simply recall here that it can be constructed from

$$S_2(\widehat{R}) = \mathrm{Span}\left\{ \frac{1}{4} \pm \frac{1}{2}x - \frac{3}{8}\left((x^2 - \frac{5}{3}x^4) - (y^2 - \frac{5}{3}y^4)\right), \right.$$
$$\left. \frac{1}{4} \pm \frac{1}{2}y + \frac{3}{8}\left((x^2 - \frac{5}{3}x^4) - (y^2 - \frac{5}{3}y^4)\right) \right\}, \qquad (8)$$

where $\widehat{R} = [-1, 1]^2$ is the reference rectangular element. Notice that this basis is just a rotation of the usual bilinear conforming basis. This form ensures that the difference of two functions belonging to NC^h is orthogonal to constants on the boundaries,[1] a characteristic used in the convergence proof. No higher spatial approximation (than using bilinear conforming elements) is gained with this rotation. The four degrees of freedom associated with $S_2(\widehat{R})$ are the values at the mid points of the faces of $\widehat{R}$, i.e., the values at the nodal points $a_1 = (-1, 0), a_2 = (0, -1), a_3 = (1, 0)$ and $a_4 = (0, 1)$. For example the basis function $\varphi_L(x, y) = \frac{1}{4} - \frac{1}{2}x - \frac{3}{8}\left((x^2 - \frac{5}{3}x^4) - (y^2 - \frac{5}{3}y^4)\right)$ is such that $\varphi_L(a_1) = 1$ and $\varphi_L(a_j) = 0$, $j = R, T, B$.

3 DISPERSION ANALYSIS: FORMULATION

In this section we set the source term to zero in Eq. (7) and restrict ourselves to a portion of the domain far away from the artificial boundaries so that we can neglect their contribution.[25, 26] Further, we assume all domains to be squares with side h. For the sake of simplicity, from now on we will omit the hat over the variables.

3.1 The analytic formulae

Let $\mathbf{k} = \mathbf{k}_r + i\,\mathbf{k}_i$ and replace p in Eq. (3) by the standing wave solution $e^{i\mathbf{k}\mathbf{x}}$. Performing some algebra, we are lead to

$$-\frac{e^{i\mathbf{k}\mathbf{x}}}{\rho(M_i - i\,M_r)}\left(|M|^2(k_r^2 - k_i^2) - \rho\omega M_r + i\,(2|M|^2 k_r k_i \cos(\theta) + \rho\omega M_i)\right) = 0, \quad (9)$$

where we have used k_r (k_i) to denote the modulus of $\mathbf{k}_r$ ($\mathbf{k}_i$), and $|M|$ to denote the modulus of the complex compressional plane wave modulus. The angle θ is the one between $\mathbf{k}_r$ and $\mathbf{k}_i$. Taking real and imaginary parts of this equation, using the imaginary part to write k_i in terms of k_r and replacing in the equation yielded by the real part, we are lead to a quartic equation for k_r. The only physically meaningful solution, and the corresponding associated k_i are

$$k_r = \frac{\sqrt{\rho\omega(M_r + \sqrt{M_r^2 + M_i^2 \sec^2(\theta)})}}{\sqrt{2}|M|},$$

$$k_i = -\frac{\sqrt{\rho}\,\omega M_i \sec(\theta)}{|M|\sqrt{M_r + \sqrt{M_r^2 + M_i^2 \sec^2(\theta)}}}. \quad (10)$$

As both quantities are real and positive, the angle θ must belong to $(\frac{\pi}{2}, \frac{3}{2}\pi)$. The boundaries of the interval can be attained only in the elastic limit.[27] Notice also that if the subsurface behaves elastically, M_i is negligible, therefore k_i also, and we recover the elastic dispersion relation, which gives $\omega/k = \sqrt{M/\rho}$. Eqs. (10) give the dispersion relations for the complex wave vector, once the compressional plane wave modulus M is replaced by the expression given in Eqs. (1)-(2).

3.2 The numeric formulae

In this section we detail the calculations leading to the numeric dispersion relations just for the nonconforming finite elements. The same procedure is followed for the conforming ones; results for both methods are shown below. To perform the dispersion analysis, we must obtain the basic algebraic equation of a typical degree of freedom.[25] In our case, such an equation involves a stencil composed of two nonconfoming elements with seven
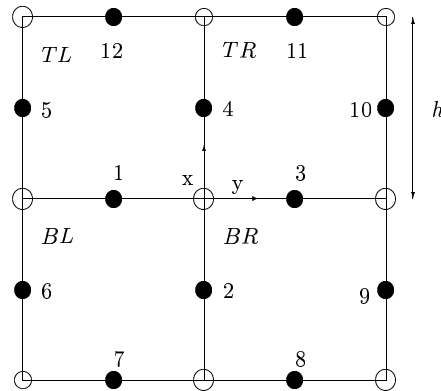
Figure 1: *Nodes involved in the calculation of the numeric dispersion relations. The black circles correspond the ones used by the NC-method, the white ones are used by the C-method. The domains utilized in the calculations are square.*

degrees of freedom. For example, the chosen degree of freedom could be the node number three and the domains TR and BR in Fig. (1). However, this stencil has a preferred orientation, and therefore does not appropriately represent the whole mesh. We must then combine two-domains stencils so as to get the smallest stencil representing the full mesh correctly, i.e., without a preferred direction.[28, 29] The resulting total number of nonconforming elements is four, involving twelve degrees of freedom. Therefore, to get the correct algebraic problem from Eq. (7) we must add the contributions of the four two-domains stencils we can form from the domains shown in Fig. 1. For example, if the two-domains stencil is $TR - BR$, $p^h = \sum_{j \in A} p_j \varphi_j$ where $A = \{2, 3, 4, 8, 9, 10, 11\}$, and the test function φ to be considered in this case is equal to φ_B in domain TR and φ_T in domain BR.

Once Eq. (7) is converted to an algrebraic problem by calculating all the integrals and adding all four partial results, we proceed to propose a function of the form $\exp(i\mathbf{k}^h\mathbf{x})$ as its solution. This expression corresponds to a standing plane wave with angular frequency ω. We situate it on the origin of coordinates, and replace the coefficients p_j, $j = 1, \ldots, 12$ accordingly. For example the coefficient associated to the node number 7 in Fig. 1 is replaced by $\exp(-ih\mathbf{k}^h(-\frac{1}{2}, 1))$. We set also $\mathbf{k}_r^h = (k_r^{1,h}, k_r^{2,h}) = (k_r^h \cos(\gamma), k_r^h \sin(\gamma))$, and similarly for $\mathbf{k}_i^h$ Of course, γ is the angle between the horizontal axis and $\mathbf{k}_r$ in the wave vectors space. After some algebraic manipulation, and separating real and imaginary

parts, we obtain a set of two coupled nonlinear equations for k_r^h and k_i^h:

$$\frac{h^2\omega^2}{3|M|^2}\left(M_r\left(\eta_1\,\eta_4{}^2\,\eta_5\,\eta_8{}^2 - \eta_1{}^2\,\eta_2\,\eta_5{}^2\,\eta_6 - \eta_1\,\eta_2{}^2\,\eta_5\,\eta_6{}^2 + \eta_2\,\eta_3{}^2\,\eta_6\,\eta_7{}^2 + \right.\right.$$

$$2\left(\eta_1\,\eta_3\,\eta_4\,\eta_5\,\eta_7\,\eta_8 + \eta_2\,\eta_3\,\eta_4\,\eta_6\,\eta_7\,\eta_8 - \eta_1\,\eta_5 - \eta_2\,\eta_6\right)\right)+$$

$$M_i\left(\eta_2{}^2\,\eta_3\,\eta_6{}^2\,\eta_7 + \eta_1{}^2\,\eta_4\,\eta_5{}^2\,\eta_8 - \eta_3{}^2\,\eta_4\,\eta_7{}^2\,\eta_8 - \eta_3\,\eta_4{}^2\,\eta_7\,\eta_8{}^2 + \right.$$

$$\left.\left.2\left(\eta_4\,\eta_8 + \eta_3\,\eta_7 + \eta_1\,\eta_2\,\eta_3\,\eta_5\,\eta_6\,\eta_7 + \eta_1\,\eta_2\,\eta_4\,\eta_5\,\eta_6\,\eta_8\right)\right)\right)+$$

$$\frac{4}{\rho}\left(-\eta_2\,\eta_6\left(-1 + \eta_9\,\eta_{13}\right) - \eta_1\,\eta_5\left(-1 + \eta_{10}\,\eta_{14}\right) + \eta_4\,\eta_8\,\eta_{11}\,\eta_{15} + \eta_3\,\eta_7\,\eta_{12}\,\eta_{16}\right) = 0,$$

$$\frac{h^2\omega^2}{3|M|^2}\left(M_r\left(\eta_2{}^2\,\eta_3\,\eta_6{}^2\,\eta_7 + \eta_1{}^2\,\eta_4\,\eta_5{}^2\,\eta_8 - \eta_3{}^2\,\eta_4\,\eta_7{}^2\,\eta_8 - \eta_3\,\eta_4{}^2\,\eta_7\,\eta_8{}^2 + \right.\right.$$

$$2\left(\eta_3\,\eta_7 + \eta_1\,\eta_2\,\eta_3\,\eta_5\,\eta_6\,\eta_7 + \eta_4\,\eta_8 + \eta_1\,\eta_2\,\eta_4\,\eta_5\,\eta_6\,\eta_8\right)\right)+$$

$$M_i\left(\eta_1{}^2\,\eta_2\,\eta_5{}^2\,\eta_6 + \eta_1\,\eta_2{}^2\,\eta_5\,\eta_6{}^2 - \eta_2\,\eta_3{}^2\,\eta_6\,\eta_7{}^2 - \eta_1\,\eta_4{}^2\,\eta_5\,\eta_8{}^2 + \right.$$

$$\left.\left.2\left(\eta_1\,\eta_5 + \eta_2\,\eta_6 - \eta_1\,\eta_3\,\eta_4\,\eta_5\,\eta_7\,\eta_8 - \eta_2\,\eta_3\,\eta_4\,\eta_6\,\eta_7\,\eta_8\right)\right)\right)-$$

$$\frac{4}{\rho}\left(\eta_3\,\eta_7\left(1 - 4\,\eta_1\,\eta_2\,\eta_5\,\eta_6 + \left(\eta_4{}^2 - \eta_2{}^2\right)\left(\eta_6{}^2 + \eta_8{}^2\right)\right)\right.$$

$$\left.+\eta_4\,\eta_8\left(1 - 4\,\eta_1\,\eta_2\,\eta_5\,\eta_6 + \left(\eta_3{}^2 - \eta_1{}^2\right)\left(\eta_5{}^2 + \eta_7{}^2\right)\right)\right) = 0, \quad (11)$$

where $\eta_1 = \cos(\frac{1}{2}hk_r^h\cos(\gamma))$, and the other expressions are shown in the appendix. This system of equations must be solved numerically.

4 ANALYSIS OF THE NUMERIC DISPERSION RELATIONS

To begin with our analysis, let us shrink the domains in the grid by making $h \to 0$ in both coordinate directions, keeping $k_{r,i}$ fixed. We can expand system (11) in terms of h, and get

$$\frac{1}{\rho}\left(k_r^2 - k_i^2\right) - \frac{\omega^2\,M_r}{|M|^2} + O(h^2) = 0,$$

$$\frac{2}{\rho}\,k_r\,k_i\,\cos(\theta) + \frac{\omega^2\,M_i}{|M|^2} + O(h^2) = 0. \quad (12)$$

Working with this expressions, we recover the analytic relations given by Eqs.(10). The same results are obtained for the system associated to the conforming finite elements, shown in the appendix.

To compare the performance of both finite element methods we use the following quantities:

$$\Xi = \frac{c^n(\omega)}{c^a(\omega)}, \qquad \Psi = \frac{|k_i^n(\omega)|}{|k_i^a(\omega)|}, \qquad \Lambda = \left(\frac{\partial\omega}{\partial k}|_{\omega_0}\right)_n\left(\frac{\partial\omega}{\partial k}|_{\omega_0}\right)_a^{-1}, \quad (13)$$

i.e., the ratio of the numeric phase velocity for each frequency (taken as $\omega/k_r(\omega)$) over the corresponding analytic one, the ratio of the numeric attenuation over the analytic one and the ratio of the numeric group velocity over the analytic one. It turns out that all quantities are independent of the frequency in the range we investigated, therefore we use just one frequency ($\omega = 100\pi$) to display our results.

In order to calculate the modulus of the numeric wave vectors (k_r^n, k_i^n) for each frequency we solve system (11) by means of Newton method, using as initial guess the analytic $\mathbf{k}$'s calculated with Eq. (10). We fix for these calculations the propagation direction γ, the angle θ between $\mathbf{k}_r$ and $\mathbf{k}_i$ and the number of points per wavelength N_p for each frequency. The domain length h is calculated as $2\pi/(N_p k_r^a(\omega))$. In all the calculations we set

$$M^r = 28.7\,10^9 N/m^2, \quad \tau_1 = \frac{1}{2\pi}10^3 s, \quad \tau_2 = \frac{1}{2\pi}10^{-6}s, \quad Q = 70, \tag{14}$$

corresponding the first value to dry Berea sandstone, and the chosen τ's ensured the corresponding constant quality factor. Our numerical experiments showed that the domain
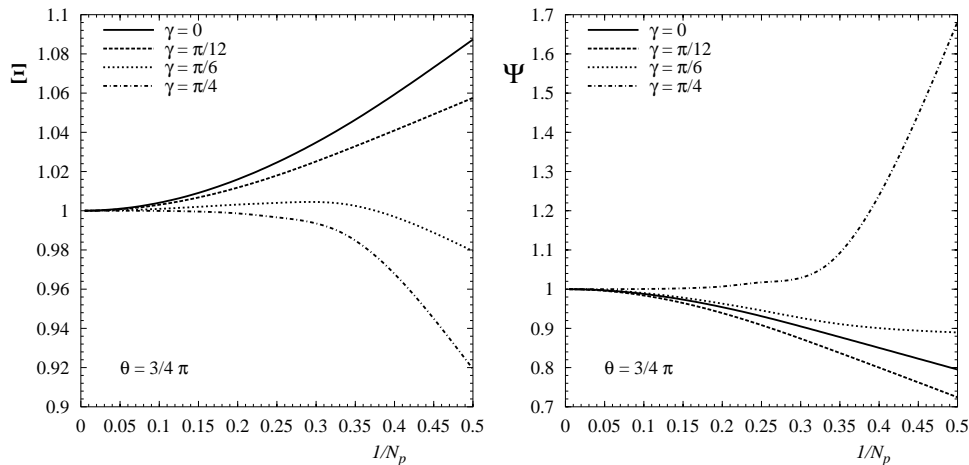

Figure 2: *Display of the results for (a) the normalized phase velocity and (b) the normalized attenuation for the NC-method, for different propagation directions, and a fixed angle between real and imaginary parts of the wave vector.*

of variation of the direction of propagation can be reduced to $[0, \pi/4]$; each solution pair (k_r^n, k_i^n) resulted to be invariant not only to reflections on the coordinate directions in the momentum space, but also to the bisectrix of the first quadrant. In Fig.2, by exemplifying with the NC-method, we show that the numerical methods introduce spatial anisotropy, because the results depend on the direction of propagation γ. This effect leads not only to a change of the phase of the wave, as in the elastic case, but also to different wave decays for different propagation directions. As expected, this misbehaviour diminish when the number of points per wavelength is increased. Notice that the apparently worst

direction is in fact the best one, because the biggest departure from one happens when about three points per wavelength are considered; until that, this curve is the one closer to the ideal behaviour. Naturally, when deciding the number of points per wavelength to use in a simulation of a real situation, the worst case is to be considered. In Fig.3
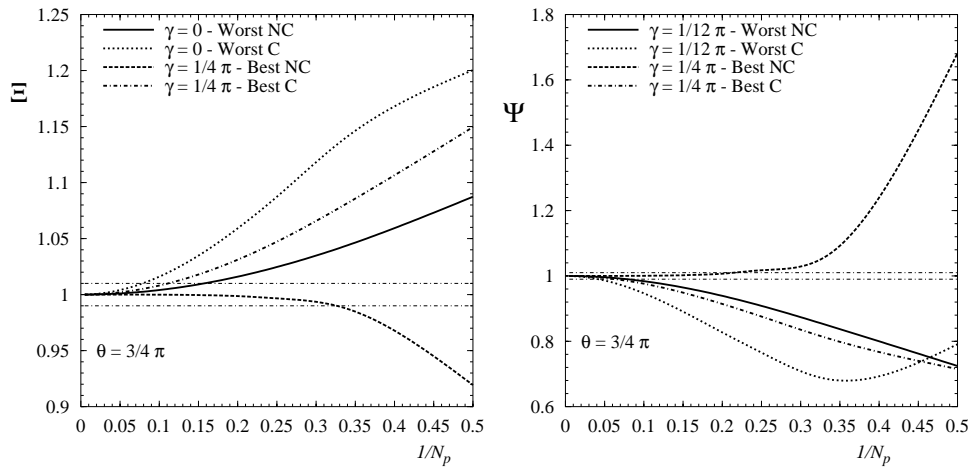

Figure 3: *Comparison of best and worst results for (a) the normalized phase velocity and (b) the normalized attenuation yielded by both methods.*

we show the best and worst behaviours for both methods. It can be observed that the NC-method performs better than the C-method; the best behaviour of the latter is still worse than the worst of the former for both the phase velocity and attenuation. In the case of the phase velocity the worst NC-method curve enters the 1% error interval -the horizontal dashed-dotted lines- at about $N_p = 10$, while the C-method needs about twice the number of points per wavelength for its worst curve to lie within the interval. When Ψ is considered, both methods need more points per wavelength to lie within the chosen error interval; in this case the difference between both methods is about six points per wavelength. In Fig.4 we show that both methods have problems when the angle θ between $\mathbf{k}_r$ and $\mathbf{k}_i$ approaches values associated to the elastic case, whenever the quality factor Q does not take correspondingly to quasi-elastic regime values. This characteristic must be taken into account for not all polarizations will be equally well modeled for a given dispersive medium. In order to avoid problems, if possible, angles θ near $\pi/2$ and π should be avoided. Notice that the NC-method behaves not as bad as the C-method, in the sense that for a fixed N_p, the distance between the lines showing good and bad behaviour is smaller for the former than for the latter. In Fig.5a we display the behaviour of the group velocity as a function of N_p, again for the NC-method. The numerator of Λ is calculated numerically using the values of k_r obtained solving system (11) to define a second order-approximate first derivative about $\omega_0 = 100\pi$, the denominator calculating the derivative of the inverse of Eq.(10) evaluated in ω_0. Again the numerical anisotropy
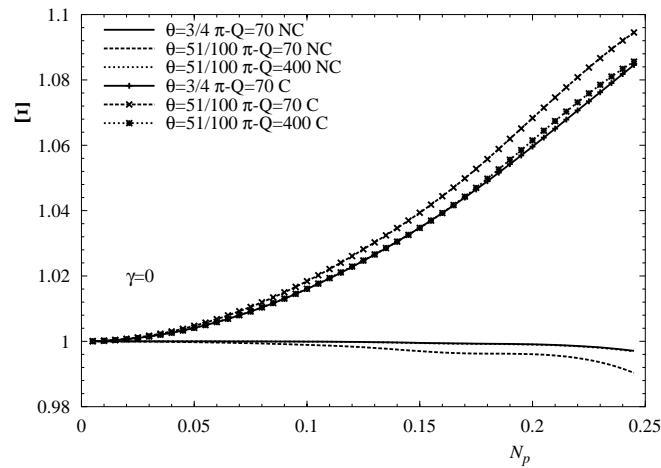
Figure 4: *Behaviour the normalized phase velocity of both methods as a function of the angle θ between real and imaginary parts of the wave vector. Note the increasing inaccuracy as $\theta \to \frac{\pi}{2}$.*
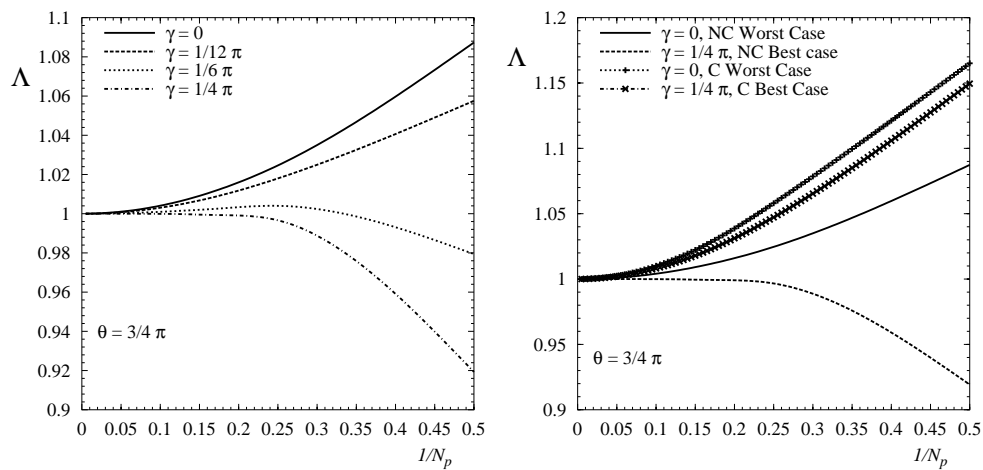

Figure 5: *Comparison of best and worst results of both methods when calculating the normalized group velocity. Note that the worst NC-method approximation is better than the best one produced by the C-method*

is apparent. In Fig.5b we show both methods best and worst results when calculating Λ. As in previous results, also for the group velocity the NC-method performs much better than the C-method; with, say, $N_p = 20$, the former has an error of .1% (.001%) and the latter of .4% (.02%) for the worst (best) directions respectively.

It can be therefore established as a rule of thumb, that the dispersion error can be calculated as the product of the error per frequency, times the number of frequencies used to transform the results back to the space-time domain. Consequently, if one desires to have a final relative errror less than, say 1 %, and is using 20 frequencies to transform from one space to another one, the number of points per wavelength N_p must be adjusted so that $20\varepsilon \leq 1\%$, where ϵ is the relative error admitted in each frequency.

5 CONCLUSIONS

We have analyzed the dispersion properties of two finite element methods, both yielding a first order spatial approximation, when applied to solve the acoustic wave equation in a dispersive medium. We have used the Liu et al. viscoelastic approximation to model the frequency-dependent dispersive properties of the soil. Just because this dispersive behaviour, it is not possible to define constant phase and group velocities -as used in the elastic case- to compare numeric with analytic results. We have therefore used frequency dependent quantities -normalized phase velocity, attenuation and group velocity-to show the numeric behaviour of the methods. We have observed that the quality of the approximations depends on the angle θ between the real and imaginary parts of the wave vector. They loose accuracy when θ takes values near the ones associated to the elastic behaviour, if correspondingly the quality factor Q is not increased. Both methods introduce numerical anisotropy, i.e., they are more or less dispersive depending on the direction of propagation considered. This leads not only to a phase difference between the numeric and analytic results -as in the elastic case- but also to a direction-dependent attenuation, due naturally to the errors introduced by the methods when approximating the imaginary part of the wave vector. In all cases studied the NC-method proved to work better than the C-method. Indeed, given a fixed accuracy requirement, using the former permits to nearly halve the number of points per wavelength required by the latter to achieve it.

REFERENCES

[1] J. Douglas, Jr., J. Santos, D. Sheen, and X. Ye. Nonconforming Galerkin methods based on quadrilateral elements for second order elliptic problems. *Mathematical Modelling and Numerical Analysis*, **33**, 744 (1999).

[2] J. Douglas, Jr., J. Santos, and D. Sheen. Nonconforming Galerkin methods for the Hemholtz equation. *Numerical Methods for Partial Differential Equations*, **17**, 475–494 (2001).

[3] A. Bayliss, C. Goldstein, and E. Turkel. On accuracy conditions for the numerical

computation of waves. *J. Comp. Phys.*, **59**, 396–404 (1985).

[4] L. L. Thompson and P. M. Pinsky. A Galerkin least squares finite element method for the two dimensional Helmholtz equation. *Int. J. Numer. Methods Eng.*, **38**(3), 371–397 (1995).

[5] F. Ihlemburg and I. Babuška. Dispersion analysis and error estimation of Galerkin finite element methods for the Helmholz equation. *Intl. J. for Numerical Methods in Engineering*, **38**, 3745–3774 (1995).

[6] F. Ihlemburg and I. Babuška. Finite element solution of the helmholtz equation with high wave number Part I: the h-version of the FEM. *Computers Math. Applic.*, **30**(9), 9–37 (1995).

[7] F. Ihlemburg and I. Babuška. Finite element solution of the helmholtz equation with high wave number Part II: the $h - p$-version of the FEM. *SIAM J. Numer. Anal.*, **34**(1), 325–358 (1997).

[8] I. Babuška and S. Sauter. Is the pollution effect of the FEM avoidable for the Helmholtz equation considering high wave numbers? *SIAM J. Numer. Anal.*, **34**(6), 2392–2423 (1997).

[9] F. Zyserman, P. Gauzellino, and J. Santos. Dispersion analysis of a non-conforming finite element method for the Helmholtz and elastodynamic equations. *Int. J. Num. Meth. Engineering, in press. Manuscript available from http://sobolev.fcaglp.unlp.edu.ar/~zyserman/2dd.ps.gz*, (2003).

[10] J.O. Blanch, J.O. Robertsson, and W.W. Symes. Viscoelastic finite difference modeling. In R. Kleinman et al., editor, *Mathematical and numerical aspects of wave propagation*, pages 69–81. SIAM, (1993).

[11] J.O.A. Robertsson, J.O. Blanch, and W.W. Symes. Viscoelastic finite-difference modeling. *Geophysics*, **59**(9), 1444–1456 (1994).

[12] T. Xu and G. A. McMechan. Efficient 3-d viscoelastic modeling with application to near-surface land seismic data. *Geophysics*, **63**(2), 601–612 (1998).

[13] T. Bohlen. Parallel 3-d viscoelastic finite difference seismic modelling. *Computers and Geosciences*, **28**, 887–899 (2002).

[14] S.M. Day and J.B Minster. Numerical simulation of wavefields using a padé approximant method. *Geophys. J. Roy. Astr. Soc.*, **78**, 105–118 (1984).

[15] H. Emmerich and M. Korn. Incorporation of attenuation into time-domain computations of seismic wave fields. *Geophysics*, **52**(9), 1252–1264 (1987).

[16] J.O. Blanch, J.O. Robertsson, and W.W. Symes. Modeling of a constant Q: Methodology and algorithm for an efficient and optimally inexpensive viscoelastic technique. *Geophysics*, **60**(1), 176–184 (1995).

[17] T. Bohlen. *Viskoelastische FD-Modellierung seismischer Wellen zur Interpretation gemessener Seismogramme*. PhD thesis, Kiel University, Germany, (1998).

[18] J.O. Blanch, J.O. Robertsson, and W.W. Symes. Viscoelastic finite difference modeling. Technical Report 93-04, Dept. of Comput. and Appl. Mathematics, Rice University, USA, (1993).

[19] I. Štekl and R. G. Pratt. Accurate viscoelastic modeling by frequency-domain finite differences using rotated operators. *Geophysics*, **63**(5), 1779–1794 (1998).

[20] M. Zener. *Elasticity and anelasticity of metals.* University of Chicago Press, (1948).

[21] R. Liu, D.L. Anderson, and H. Kanamori. Velocity dispersion due to anelasticity: implications for seismology and mandtel composition. *Geophys. J. Roy. Astr. Soc.*, **47**, 41–58 (1976).

[22] J. Carcione. *Wave fields in real media: Wave propagation in anisotropic, anelastic and porous media*, volume 31 of *Handbook of Geophysical Exploration.* Pergamon Press, (2001).

[23] P. Gauzellino, J. Santos, and D. Sheen. Frequency domain wave propagation modeling in exploration seismology. *Journal of Computational Acoustics*, **9**(3), 941–955 (2001).

[24] J. Douglas, Jr., J. Santos, and D. Sheen. Approximation of scalar waves in the space-frequency domain. *Mathematical methods and models in applied sciences*, **4**, 509 (1994).

[25] A. Bamberger, G. Chavent, and P. Lailly. Etude de schémas numériques pour les équations de l élastodynamique linéaire. Technical Report 41, INRIA, (1980).

[26] K.J. Marfurt. Accuracy of finite-difference and finite-element modelling of the scalar and elastic wave equations. *Geophysics*, **49**, 533 (1984).

[27] J. A. Hudson. *The excitation and propagation of elastic waves.* Cambridge University Press, (1980).

[28] I. Babuška. *International journal for numerical methods in engineering*, **37**, 1073 (1994).

[29] C. Farhat, I. Harari, and U. Hetmaniuk. A discontinuous Galerkin method with Lagrange multipliers for the solution of Helmholtz problems in the mid-frequency regime. *Computer methods in applied mechanics and engineering*, **192**, 1389–1419 (2003).

A   APPENDIX

The analog to system of equations (11) corresponding to the C-method is

$$\frac{h^2\omega^2}{9|M|^2}\left(M_r\left(-4-2\,\eta_9\,\eta_{13}-2\,\eta_{10}\,\eta_{14}-\eta_9\,\eta_{10}\,\eta_{13}\,\eta_{14}+\eta_{11}\,\eta_{12}\,\eta_{15}\,\eta_{16}\right)+\right.$$
$$\left.M_i\left(2\,\eta_{11}\,\eta_{15}+2\,\eta_{12}\,\eta_{16}+\eta_{10}\,\eta_{11}\,\eta_{14}\,\eta_{15}+\eta_9\,\eta_{12}\,\eta_{13}\,\eta_{16}\right)\right)-$$
$$\frac{2}{3\rho}\left(-4+\eta_{10}\,\eta_{14}+\eta_9\,\eta_{13}\left(1+2\,\eta_{10}\,\eta_{14}\right)-2\,\eta_{11}\,\eta_{12}\,\eta_{15}\,\eta_{16}\right)=0,$$
$$\frac{h^2\omega^2}{9|M|^2}\left(M_r\left(2\,\eta_{11}\,\eta_{15}+2\,\eta_{12}\,\eta_{16}+\eta_{10}\,\eta_{11}\,\eta_{14}\,\eta_{15}+\eta_9\,\eta_{12}\,\eta_{13}\,\eta_{16}\right)+\right.$$
$$M_i\left(4+2\,\eta_9\,\eta_{13}+2\,\eta_{10}\,\eta_{14}+\eta_9\,\eta_{10}\,\eta_{13}\,\eta_{14}-\eta_{11}\,\eta_{12}\,\eta_{15}\,\eta_{16}\right)\right)+$$
$$\frac{2}{3\rho}\left(\eta_{11}\,\eta_{15}\left(1+2\,\eta_{10}\,\eta_{14}\right)+\eta_{12}\,\eta_{16}\left(1+2\,\eta_9\,\eta_{13}\right)\right)=0. \quad (15)$$

The expressions for the ηs are the following:

$$\eta_1 = \cos(\tfrac{1}{2}k_r^h h\cos(\gamma)), \qquad \eta_2 = \cos(\tfrac{1}{2}k_r^h h\sin(\gamma)),$$
$$\eta_3 = \sin(\tfrac{1}{2}k_r^h h\cos(\gamma)), \qquad \eta_4 = \sin(\tfrac{1}{2}k_r^h h\sin(\gamma)),$$
$$\eta_5 = \cosh(\tfrac{1}{2}k_i^h h\cos(\gamma+\theta)), \qquad \eta_6 = \cosh(\tfrac{1}{2}k_i^h h\sin(\gamma+\theta)),$$
$$\eta_7 = \sinh(\tfrac{1}{2}k_i^h h\cos(\gamma+\theta)) \qquad \eta_8 = \sinh(\tfrac{1}{2}k_i^h h\sin(\gamma+\theta))$$
$$\eta_9 = \cos(k_r^h h\cos(\gamma)), \qquad \eta_{10} = \cos(k_r^h h\sin(\gamma)),$$
$$\eta_{11} = \sin(k_r^h h\cos(\gamma)), \qquad \eta_{12} = \sin(k_r^h h\sin(\gamma)),$$
$$\eta_{13} = \cosh(k_i^h h\cos(\gamma+\theta)), \qquad \eta_{14} = \cosh(k_i^h h\sin(\gamma+\theta)),$$
$$\eta_{15} = \sinh(k_i^h h\cos(\gamma+\theta)) \qquad \eta_{16} = \sinh(k_i^h h\sin(\gamma+\theta)). \quad (16)$$